ACSES *proceedings*

2010

Computational Analysis of Vortex Dynamics in One-Component Bose-Einstein Condensates

Eunsil Baik and Ricardo Carretero-Gonzalez

AP10-01

CSRC gateway to the future an interdisciplinary

San Diego State University

Computational Analysis of Vortex Dynamics in One-Component Bose-Einstein Condensates

Eunsil Baik[1] *and Ricardo Carretero-González*[2]
[1]*San Diego State University,* [2]*San Diego State Univeristy*
[1]*ebaik@sciences.sdsu.edu,* [2]*carreter@sciences.sdsu.edu*

Abstract: We consider the Gross-Pitaeviskii Equation (GPE) to describe the dynamics of vortices in one-component BECs. In order to solve GPE, we use the 2nd order central finite difference scheme for the spatial derivation and the 4th order Runge-Kutta method to integrate in time. For a vortex wave function, we solve the well known vortex profile ODE numerically. With different external potentials, we observe different dynamics of vortices in BECs such as the vortex drift on a plane potential with an angle, the vortex-vortex interaction on a plane field with the same vorticity and the opposite vorticity, and the vortex precession on a magnetic trap potential. Our computational analysis observes all different vortex dynamics, and it confirms and supports the theoretical analysis that has been done previously.

Keywords: BECs, Thomas-Fermi, fluid velocity

1 Introduction

Bose-Einstein condensates (BECs) are a quantum state of dilute atomic gases of weakly interacting bosons confined in an external potential and cooled to temperatures near absolute zero. The theory BECs was initiated in 1924-1925 [5, 6] and it was not experimentally observed in dilute atomic gases until 1995 [2]. Ever since the first observation of the BEC was made by JILA in 1995, it has been a very popular subject to many theorists and experimentalist, and it has been studied intensely. As in many other systems, vortices could be formed in the BECs. One could create vortices by engineering the condensate with lasers or by rapidly rotating the confining trap. Many works have studied the dynamics of vortices in BECs in detail and formulas describing the approximative motion of the vortex have been reported [17, 21, 9, 16, 1, 18, 11, 20].

The actual experiment done by JILA was using two-component condensates of atomic gas ^{87}Rb [1]. In this computational work, we study the vortex dynamics in one-component BECs. For the comparison, various theories about the motion of the vortex in BECs are evaluated. In Sec. 2 we describe the equations of the motion of a vortex in a BEC as well as the vortex profiles. In Sec. 3, the numerical techniques that are used to perform the computational simulations are introduced, and in Sec. 4, different external potentials are introduced and the numerical results of the vortex dynamics are compared with the theory. Finally, we summarize the results and give possible future work directions.

2 Equations of Motion

The most appropriate way to describe the meanfield dynamics near absolute zero of a BEC is the Gross-Pitaevskii equation (GPE). The GPE gives a very good description of the dynamics in BECs. The generic GPE describing the evolution of the condensate wave function Ψ is:

$$i\hbar\frac{\partial\Psi}{\partial t} = -\frac{\hbar^2}{2M}\boldsymbol{\nabla}^2\Psi + V(x,y,z)\Psi + g_{3D}\left|\Psi\right|^2\Psi, \tag{1}$$

where $\hbar$ is the Planck's constant, M is the mass of the bosons, $V(x,y,z)$ is the external potential, and $g_{3D} = 4\pi\hbar^2 a/M$ is the coupling constant for the full 3-dimensional GPE where a is the s-wave scattering length.

When the BEC density grows from 0 to ρ over the distance ξ, the kinetic energy ($\backsim \hbar^2/2M\xi^2$) and the interaction energy ($\backsim 4\pi\hbar^2 a\rho/M$) become equal at the value $\xi = 1/\sqrt{8a\pi\rho}$ and this ξ is named 'healing length'.

To simplify the computational simulations, the GPE that is used for the actual numerical simulations is:

$$i\frac{\partial\Psi}{\partial t} = -\frac{1}{2}\nabla^2\Psi + V(x,y)\Psi + g\,|\Psi|^2\,\Psi. \quad (2)$$

When there is no external potential, Eq. (2) becomes:

$$i\Psi_t + \frac{1}{2}\nabla^2\Psi - g|\Psi|^2\Psi = 0. \quad (3)$$

Now we consider the steady solution to the GPE as:

$$\Psi(r,\theta) = u(r)e^{-i\mu t}e^{iS\theta}, \quad (4)$$

where S is the charge of the vortex (or vorticity) and θ is the polar angle measure from the center of the vortex. Changing Euclidean coordinates to polar coordinates, the Laplace operator transforms to:

$$\nabla^2 = \frac{1}{r}\frac{\partial}{\partial r}\left(r\frac{\partial}{\partial r}\right) + \frac{1}{r^2}\frac{\partial^2}{\partial\theta^2}. \quad (5)$$

Using the Laplacian operator (5) in Eq. (3) with the ansatz (4), the vortex profile equation is given by:

$$\mu u + \frac{1}{2}\left[u'' + \frac{1}{r}u' - \frac{S^2}{r^2}u\right] - gu^3 = 0. \quad (6)$$

This is a boundary value problem that has no analytical closed solution and the boundary conditions are $u(0) = 0$ and $u'(\infty) = 0$. However, an approximate solution can be given in terms of tanh. Consequently, we use $u(r) = \tanh(r)$ as an initial guess for the solution. This ordinary differential equation is solved using Matlab built-in BVP function. The initial guess and the solutions for different charges are shown in Fig. 1.

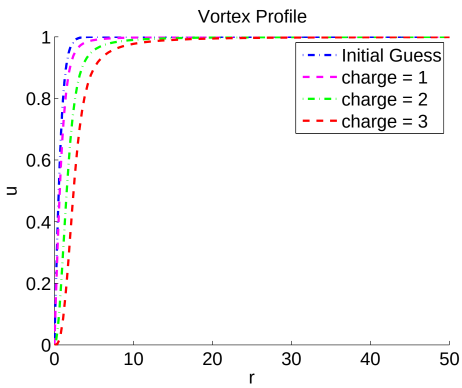

Figure 1: Vortex profiles for different vortex charges. The x-axis is the polar length r and the y-axis shows the vortex amplitude $u = |\Psi|$.

3 Numerical Analysis

For the numerical analysis, we start from the steady state solution of the GPE. From the modified 2-dimensional GPE (2) with the kinetic term neglected (Thomas-Fermi approximation), the reduced form of the equation reads:

$$i\frac{\partial\Psi}{\partial t} = V(x,y)\Psi + g\,|\Psi|^2\,\Psi. \quad (7)$$

By substituting the ansatz (4) into Eq. (7) and simplifying, we obtain:

$$\mu u = Vu + u^3. \quad (8)$$

From Eq. (8), we set the initial condition of the wave function Ψ as:

$$\Psi_0 = \sqrt{\frac{\max(\mu - V, 0)}{g}} \quad (9)$$

To seed a vortex, we change the radial vortex profile $u(r)$ into cartesian coordinates $u(x,y)$ and form a product of all terms: the initial wave function Ψ_0, the cartesian coordinates vortex profile $u(x,y)$, and the phase term $e^{iS\theta}$. The final form of the wave function reads as following:

$$\Psi = \Psi_0 \cdot u(x,y) \cdot e^{iS\theta}. \quad (10)$$

With a magnetic trap as an external potential, we use the Newton method to find the (numerically) exact background profile.

Once the initial background is found, to seed vortices on this background, the vortex profile is multiplied to the initial background. The vortex profile is in one-dimensional radial (r) coordinates as shown in Fig. 1. From this, on a set domain of X and Y, we use the Matlab built-in function `spline` to fit this radial profile into the two-dimensional setup (to wrap around in 360 degrees on the xy-planal coordinates).

For the second order spatial differential part of the GPE, the second order central finite difference scheme is used. To integrate the system in time, the 4th order Runge-Kutta method is used. While integrating the system for each time step, every predetermined number of steps a solution is saved and the vorticity fitting is done. Using the vorticity, the path of the vortex can be computed. The vorticity is given in terms of the fluid velocity.

$$\vec{w} = \nabla \times \vec{v}, \tag{11}$$

where v is the fluid velocity

$$\vec{v}_{fluid} \equiv \frac{\Psi \nabla \Psi^* - \Psi^* \nabla \Psi}{i\,|\Psi|^2}, \tag{12}$$

where Ψ is the wave function of the system. To compute this fluid velocity numerically, one needs to modify the formula since where the density of the wave function $|\Psi|^2$ is zero, the formula has zero in the denominator that cannot be computed numerically. To avoid having zero density in the denominator of the fluid velocity (or to smooth the peak of vorticity), we add a small numerical parameter δ in the denominator of Eq. (12):

$$\vec{v}_{fluid} \equiv \frac{\Psi \nabla \Psi^* - \Psi^* \nabla \Psi}{i\left(|\Psi|^2 + \delta\right)}. \tag{13}$$

With this smoothing parameter $\delta = 1.0$, we have the peak of vorticity less sharp and this makes much convenient to do the best fitting of the vorticity. This vorticity computation is used to follow the vortex to study how the vortex moves in a particular background.

4 Numerical Results and Comparison

4.1 Vortices on Plane Potentials

For a plane potential, one can think of the external potential to be flat and extending infinitely. Consequently, the BEC steady state density would be an infinite plane with some slope. When the slope is zero and the vortex is sitting at the center of the plane, for there is no trigger to start the dynamics, there is no movement of the vortex. However, if the plane is tilted at a certain angle (we call this the slope of the potential), the gradient of the background field will initiate the dynamics of the vortex [13, 14, 10, 3], so that the vortex moves perpendicular to the gradient of the background field. In addition to the effect from the gradient of the background field, the mirror images due to the boundary conditions affect the vortex dynamics as well [11, 20].

4.1.1 Vortex Drift

To initiate the vortex dynamics, we start with a tilted plane potential. Since the initiating factor is the gradient of the background field, as the angle of tilt increases, the linear velocity of the vortex increases. The analytical formula for this velocity is obtained from Kivshar et al. [10] as:

$$k_0 n_0 \frac{\mathrm{d}\mathbf{r}_0}{\mathrm{d}z} = \left(-\nabla\theta_b + \frac{S}{2} C \mathbf{J} \nabla \ln I_b\right)\Bigg|_{r=r_0}, \tag{14}$$

where k_0 is the free-space wave number, n_0 is the linear refractive index, $\mathbf{r}_0$ is the center coordinates of a vortex, θ_b is the phase of the background field, S is the vortex charge (polarity), I_0 is the intensity of the background field, $\mathbf{J}$ is the matrix operation of rotation by $\pi/2$, and C is a function of I_b. In the particular case of a Kerr medium, the coefficient C has been derived in Ref. [10] as:

$$C = -\ln\left(\frac{c e^{\gamma}\,|\nabla \ln \mathbf{I}_b|}{4 k_0 n_0 \sqrt{2 n_2 I_0 / n_0}}\right), \tag{15}$$

with $c \approx 1.126$ is a constant value numerically computed in Ref. [10], γ is the Euler's constant ($\gamma \approx 0.557$), and n_2 is the nonlinear refractive index.

In order to compare the validity of Eq. (14) with our computational results, a few substitutions have been made to have an equivalent system of equations as our modified GPE:

$$\begin{aligned} k_0 &= 1, \\ n_0 &= -1, \\ n_2 &= -1. \end{aligned}$$

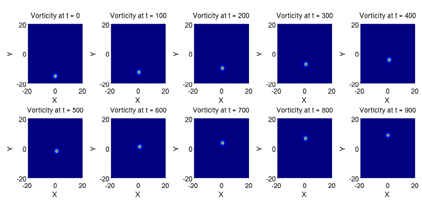

Figure 2: Vorticity plot of a vortex on a plane potential with the slope $m = 0.01$. The initial position of the vortex is $(0, -15)$ and the final position at time $t = 1000$ is at $(0, 11.5187)$.

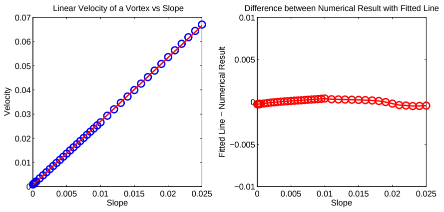

Figure 3: Left: vortex velocity vs. slope of plane potential. The slope varies from 0.0005 to 0.025. The plot shows the velocity that depends linearly as the slope (see the linear fit depicted by the solid line). Right: plot shows the difference between the numerical result and its linear fit.

For the computational simulations, we start with the steady solution to the GPE with the plane potential $V = m \cdot X$, where m represents the slope or tilt of the potential plane. With this steady state solution, we multiply the vortex profile to have a vortex sitting on the plane background field. Since the tilt is in X-direction, we expect to have a movement of the vortex in Y-direction. If a vortex is initially seeded at $(0, -15)$ and the slope of the plane potential is $m = 0.01$ (see Fig. 2), the velocity of the vortex is computed by doing the best fitted line to the trajectory of the vortex and it is found to be $v_N = 0.0266$, while its theoretical value is $v_T = 0.0282$. The initial position of the vortex for all our runs is $(0, -15)$ and the size of domain is $X = (-50, 50)$. As for the first comparison of the linear velocity of a BEC vortex with a plane potential, we took varied slopes from 0.001 to 0.01. The numerical results are slightly less than the theoretical results (from formula by Kivshar et al. [10]). Using the numerical data and the theoretical formula, a curve has been fitted to the data giving a constant c value of 1.9656, while the value from theoretical formula is 1.126. For the second comparison of the linear velocity of a BEC vortex with a plane potential, we took varied slopes from 0.01 to 0.025. The numerical results were slightly less than the theoretical results in the beginning, and then the numerical results became greater than the theoretical results (from formula by Kivshar et al. [10]). Using numerical data and the theoretical formula, a curve has been fitted to the data giving a constant c value of 0.78069. The numerical results are similar to the theoretical results, but they are not exactly the same. There is a factor c in Kivshar's formula, which was computed by doing the numerical integration. By applying the least square analysis we obtain a modified value for the c constant that better fits our data. Nevertheless, the velocity of a vortex depends linearly on the angle of the plane potential and our numerical result shows a proper linear dependency of the velocity to its plane potential angle (see Figs. 3).

4.1.2 Vortex-Vortex Interaction

When there is no slope in the external potential and having two vortices in one-component BEC, the phase gradient initiates the dynamics. Same charge (or same vorticity) vortices move in a circular orbiting motion; whereas, with opposite charge they move in a line parallel to each other. From this, we find the velocity of a vortex induced by another vortex. In addition, the velocity depends on the separation distance between the vortices.

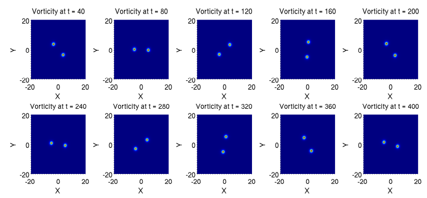

Figure 4: Vorticity plot of the same charge vortex-vortex interaction in its absence of background potential gradient. The initial position of one vortex is at $(0, -5)$ and the initial position of the other vortex is at $(0, 5)$.

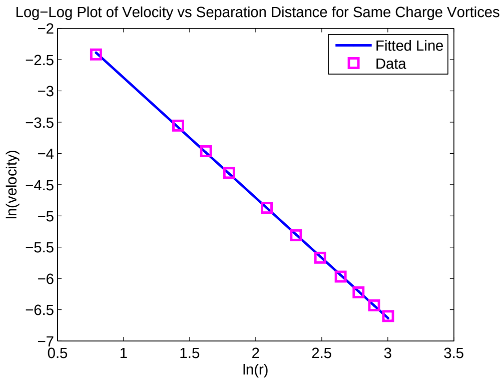

Figure 5: Same charge vortex-vortex interactions at different separation distances between two vortices. A log-log plot of the angular velocity as a function of the separation distance. As the separation distance between two vortices changes from 4 to 40 the vortex rotates at a faster rate.

In the case of same charge vortices, we follow the trajectory of the vortex. From this trajectory we compute the angle of rotation using the `atan2` function at each time. The angle vs. time is fitted and the slope of this line represents the angular velocity of the vortex. An example of the same charge vortex-vortex interaction is shown in Fig. 4. Both vortices have charge of $+1$ and their separation distance is 10. The size of domain is $X = (-50, 50)$ with the spatial step size $dx = 0.4$ and the time step size $dt = 0.1$. By varying the separation distance between these two vortices, we obtain different angular velocities. Fig. 5 shows the log-log plot of the angular velocity vs. separation distance.

In the case of the opposite charge vortices, the position of the vortices is fitted to the best line and the slope of that line gives the linear velocity of the vortices. An example of the opposite charge vortex-vortex interaction is shown in Fig. 6. One vortex has charge of $+1$ and the other has charge of -1. The separation distance is 10 with domain of size $X = (-50, 50)$. The spatial step size is $dx = 0.4$ and the time step $dt = 0.1$. Different separation distances between these two vortices give different velocities as depicted in Fig. 7.

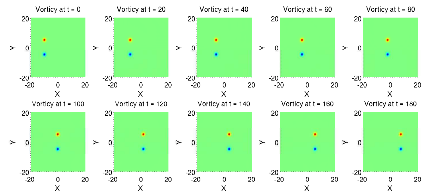

Figure 6: Vorticity plot of the opposite charge vortex-vortex interaction in the absence of the external potential. The initial position of one vortex is at $(-15, -5)$ and the initial position of the other vortex is at $(-15, 5)$.

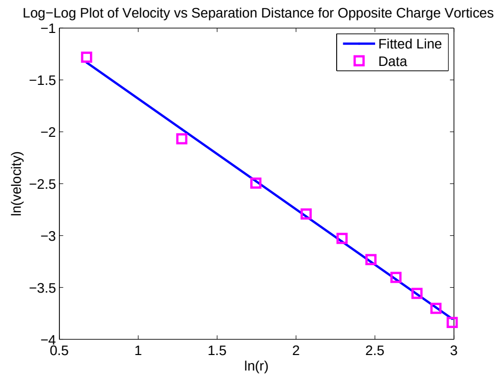

Figure 7: Opposite charge vortex-vortex interactions at different separation distances between two vortices. A log-log plot of the linear velocity as a function of the separation distance. As the separation distance between two vortices changes from 4 to 40 the vortex moves at a faster rate.

4.2 Vortices on Magnetic Trap

The most interesting phenomena happen with a vortex in a magnetic trap external potential. Many formulas have been found to describe the motion of the vortex in this Thomas-Fermi (TF) cloud. Lundh et al. [11] give a formula for the vortex dynamics in the TF cloud that takes into account the gradient of the background field and the mirror image effect produced at the edge of the condensed cloud. Consequently, the formula has two parameters that affect the vortex dynamics: the frequency (i.e. strength) of the trap ω and the distance of the vortex from the center of the TF cloud r_0. The angular velocity Ω is:

$$\Omega = \frac{\hbar}{2MR^2\left(1 - \dfrac{r_0^2}{R^2}\right)} g(r_0/R), \qquad (16)$$

with

$$g(x) = 2\ln\left(\frac{R}{\xi}\right) + \left(\frac{1}{x^4}\right)\ln(1-x^2) + \frac{1}{x^2} + 2, \tag{17}$$

and the local healing length ξ is

$$\xi(r_0) = \frac{1}{\sqrt{8\pi u(r_0)a}} = \frac{\xi_0}{\sqrt{1 - r_0^2/R^2}}, \tag{18}$$

where $\hbar$ is the Planck's constant, R is the TF radius $R = (2\mu/M\omega^2)^{1/2}$ where ω is the trap frequency, M is the mass of bosons, and r_0 is the initial location of the vortex from the center of the TF cloud. To have this formula equilvalent to our system we set $\hbar = 1$ and $M = 1$.

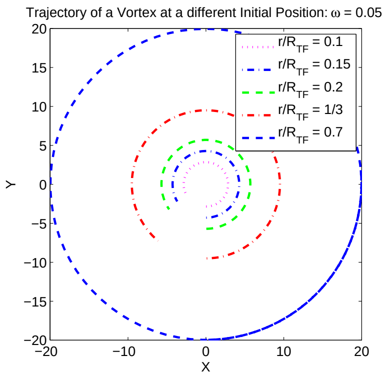

Figure 8: Vortex precession in the TF cloud with the trap frequency $\omega = 0.05$. The trajectory shows for each vortex precession for the ratio r/R is from 0.1 to 0.7. As the initial position of the vortex is close to the edge of TF cloud, the angular velocity increases.

Another formula is found in Fetter et al. [20] where it is assumed that the vortex is sitting near the center of the TF cloud. Consequently, the only parameter for this formula is the frequency of a trap ω. The angular velocity Ω is:

$$\Omega = \mp\frac{3\hbar\omega_x\omega_y}{4\mu}\ln\frac{R}{\xi}, \tag{19}$$

where $\hbar$ is the Plank's constant, μ is the chemical potential (in our system, $\mu = 1$), R is the TF radius, ω_x and ω_y are the trap frequencies along the x and y directions respectively (they are equal in our system $\omega_x = \omega_y = \omega$), and $\xi = \hbar/\sqrt{2M^2}$ is the healing length.

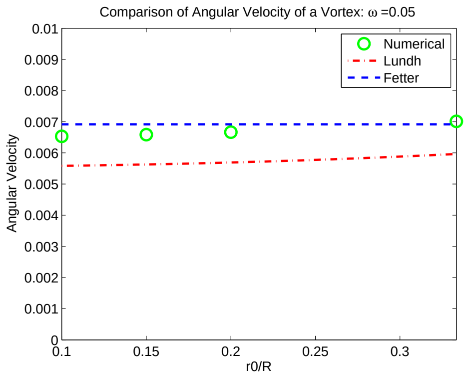

Figure 9: A plot of comparison between the numerical result and the theoretical results when $\omega = 0.05$. For each different trap frequency ($\Omega = 0.2$, 0.3, 0.4, and 0.5), the angular velocity of the vortex is compared with the theoretical prediction (see text) at varied ratio of r/R. Since the formula by Fetter et al. [20] does not depend on the initial position of the vortex, it does not vary at different ratio r/R (shown as a horizontal line). However, the formula by Lundh et al. [11] depends on the initial position of the vortex and it varies at different ratio r/R.

As before, we start with the steady state solution with a magnetic trap external potential $V = \frac{1}{2}\omega^2\left(X^2 + Y^2\right)$. After 'cleaning' the TF approximation using the Newton's method, we seed a vortex some distance from the center at $(0, Y_0)$, where $Y_0 = -fact \cdot R_{TF}$, R_{TF} is the radius of TF cloud, and *fact* is varied. One example of the resulting precession induced by the magnetic trap is shown in Fig. 8. This plot shows the vortex precession for different initial positions when the frequency of the trap is fixed at $\omega = 0.05$. The parameters that are controlled are the frequency of the trap ω and the distance of the vortex from the center, r. For different values of ω ($\omega = 0.02$, 0.03, 0.04, and 0.05), we had several runs for different distances from the center. The distance of the vortex from the center was recorded as the ratio of the distance of the vortex from the center of the TF cloud and the radius of the TF cloud $fact = r/R_{TF}$ and the values of *fact* are 0.1, 0.15, 0.2, 1/3, and 0.7. As expected, due to the mirror image effect, as a vortex goes near the boundary (when *fact* is 1/3 or 0.7), the angular velocity increases.

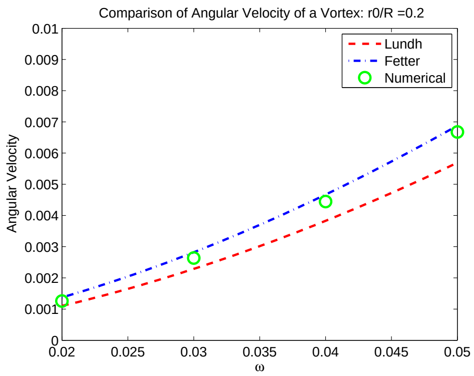

Figure 10: A plot of the comparison between the numerical result and the theoretical results when the ratio $r/R = 0.2$. For each ratio of the initial position of the vortex and the size of trap, $r/R = 0.1$, 0.15, 0.2, and 1/3, the angular velocity of the vortex is compared with the theoretical at different trap frequencies. Both theoretical formulas depend on the trap frequency; consequently, the angular velocity varies depending on the trap frequency.

Once the angular velocities are found, they are compared with the analytical formulas such as Lundh et al. [11] and Fetter et al. [20] (labeled as *Lundh* and *Fetter* respectively). Plots of the comparison for each value of ω are shown in Fig. 9. Our computational angular velocities lie between these two theoretical angular velocities as expected since Lundh's formula takes account of the mirror image effect and Fetter's formula does not. Furthermore, since Fetter's formula only depends on the frequency of the trap, it has the same angular velocity with varied ratio r/R; whereas, Lundh's formula gives the different angular velocity for each different ratio. In addition to the comparison for each ω, plots of the comparison for each *fact* ratio are shown in Fig. 10. Our computational angular velocities lie between these two theoretical angular velocities when the ratio is relatively smaller, and then the computational one is much closer to Fetter's formula.

5 Conclusions

On this paper, we have analyzed the vortex dynamics in one-component Bose-Einstein condensates (BECs) which shows a very good agreement with the previous theoretical analysis [11, 20, 10]. The formula by Kivshar et al. [10] comes from optics with numerically to-be-determined numerical constant value and coefficient. Our computational analysis shows a proper linear relationship between the vortex velocity and the angle of tilt of the external plane potential. For vortex-vortex interactions, the numerical simulations confirm the theoretical expectations such as the linear velocities for the opposite charge vortex-vortex interaction and the angular velocities for the same charge vortex-vortex interaction. With a magnetic trap as an external potential, we computed the angular velocity of the vortex for different trap frequencies and for different initial positions of the vortex. By comparing two theoretical formulas by Lundh et al. [11] and Fetter et al. [20], we showed that our numerical simulation agrees with these theoretical formulas. The next step to this study will be the computational analysis of vortex dynamics in two-component BECs [4, 7, 15, 12, 8, 19]. For two-component BECs, we would need to formulate the condensate with two coupled Gross-Pitaevskii equations (GPEs). With two coupled GPEs, we have intra-species coupling constants within each component, inter-species coupling constants between two components, and linear coupling constants between two components.

References

[1] B. P. Anderson, P. C. Haljan, C. E. Wieman, , and E. A. Cornell, *Vortex precession in bose-einstein condensates: Observations with filled and empty cores*, Phys. Rev. Lett. **85** (2000), no. 14.

[2] M. H. Anderson, J. R. Ensher, M. R. Matthews, C. E. Weiman, and E. A. Cornell, *Observation of bose-einstein condensation in a dilute atomic vapor*, Science, New Series **269** (1995), no. 5221, 198–201.

[3] J. R. Anglin, *Vortices near surfaces of bose-einstein condensates*, Phys. Rev. A **65** (2002), no. 063611.

[4] B. Apagyi and D. Schumayer, *Assessment of interspecies scattering lengths a_{12} from stability of two-component bose-einstein condensates*, Eur. Phys. J. B **45** (2005), 55–61.

[5] S. N. Bose, *Plancks gesetz und lichtquantenhypothese*, Zeitschrift für Physik **26** (1924), 178–181.

[6] A. Einstein, *Quantentheorie des einatomigen idealen gases*, Sitzungsber Preuss Akad Wiss **1** (1924), no. 3, 261–267.

[7] A. Gubeskys, B. A. Malomed, and I. M. Merhasin, *Two-component gap solitons in two- and one-dimensional bose-einstein condensates*, Phys. Rev. A **73** (2006), no. 023607.

[8] David S. Hall, *Multi-component condensates: Experiment*, Springer Series on Atomic, Optical, and Plasma Physics **45** (2008), no. 3, 307–327.

[9] B. Jackson, J. F. McCann, and C. S. Adams, *Vortex line and ring dynamics in trapped bose-einstein condensates*, Phys. Rev. A **61** (1999), no. 013604.

[10] Yuri S. Kivshar, Jason Christou, Vladimir Tikhonenko, Barry Luther-Davies, and Len M. Pismen, *Dynamics of optical vortex solitons*, Optics Communications **152** (1998), 198–206.

[11] Emil Lundh and P. Ao, *Hydrodynamics approach to vortex lifetimes in trapped bose condensates*, Phys. Rev. A **61** (2000), no. 063612.

[12] Boris Malomed, *Multi-component bose-einstein condensates: Theory*, Springer Series on Atomic, Optical, and Plasma Physics **45** (2008), 287–306.

[13] Peter Mason and Natalia G. Berloff, *Motion of quantum vortices on inhomogeneous backgrounds*, Phys. Rev. A **77** (2008), no. 032107.

[14] Peter Mason, Natalia G. Berloff, and Alexander L. Fetter, *Motion of a vortex line near the boundary of a semi-infinite uniform condensate*, Phys. Rev. A **74** (2006), no. 043611.

[15] M. R. Matthews, B. P. Anderson, P. C. Haljan, D. S. Hall, C. E. Wieman, and E. A. Cornell, *Vortices in a bose-einstein condensate*, Phys. Rev. Lett. **83** (1999), no. 13.

[16] S. A. McGee and M. J. Holland, *Rotational dynamics of vortices in confined bose-einstein condensates*, Phys. Rev. A **63** (2001), no. 043608.

[17] B. Y. Rubinstein and L. M. Pismen, *Vortex motion in the spatially inhomogeneous conservative ginzburg-landau model*, Physica D **78** (1994), 1–10.

[18] Daniel E. Sheehy and Leo Radzihovsky, *Vortices in spatially inhomogeneous superfluids*, Phys. Rev. A **70** (2004), no. 063620.

[19] Hua Shi, Hadi Rastegar, and A. Griffin, *Bose-einstein condensation of a coupled two-component bose gas*, Phys. Rev. E **51** (1995), no. 2.

[20] Anatoly A. Svidzinsky and Alexander L. Fetter, *Stability of a vortex in a trapped bose-einstein condensate*, Phys. Rev. Lett. **84** (2000), no. 26.

[21] J. Tempere and J. T. Devreese, *Vortex dynamics in a parabolically confined bose-einstein condensate*, Solid State Communications **113** (2000), 471–474.